Pattern formation of Rayleigh-Bénard convection of cold water near its density maximum in a vertical cylindrical container

You-Rong Li,* Yu-Qing Ouyang, and Yu-Peng Hu
Key Laboratory of Low-Grade Energy Utilization Technologies and Systems of Ministry of Education, College of Power Engineering, Chongqing University, Chongqing 400044, China
(Received 18 April 2012; revised manuscript received 30 June 2012; published 31 October 2012)

In order to understand the onset of convective instability and multiple stable convection patterns of buoyancy-driven convection of cold water near its density maximum in a vertical cylindrical container heated from below, a series of three-dimensional numerical simulations were performed. The aspect ratio of the container was 2 and Prandtl number of cold water was 11.57. The sidewall was considered to be perfectly adiabatic, and the density inversion parameter was fixed at 0.3. The result shows that the density inversion phenomenon in cold water has an important effect on the critical Rayleigh number for the onset of convection and the pattern formation at higher Rayleigh numbers. When the Rayleigh number varies from 3×10^3 to 1.2×10^5, eight stable, steady convection patterns are obtained under different initial conditions. The coexistence of multiple stable steady flow patterns is also observed within some specific ranges of the Rayleigh number.

DOI: 10.1103/PhysRevE.86.046323 PACS number(s): 47.20.Ky, 47.20.Bp, 47.54.−r, 65.40.De

I. INTRODUCTION

Rayleigh-Bénard convection in confined enclosures is an important problem due to its practical applications in engineering and science, and for its theoretical aspect of being a simple system for the study of complex pattern formation and the rich dynamical behavior of high-dimensional nonlinear systems. During the past few decades, many experimental observations [1–4], theoretical analyses [5–7], and numerical simulations [8–12] have been reported on the occurrence of various convective patterns in cylinders for the Boussinesq fluid with a linear temperature-dependent density. From those remarkable works, it has become well known that the motionless conductive state will lose its stability and bifurcate to the convection when the Rayleigh (Ra) number exceeds a critical value, which depends on the aspect ratio (Γ = radius/height) and the sidewall conductivity of the enclosure. As the Rayleigh number is increased above the onset, the fluid motion becomes highly nonlinear and leads to complex spatial and temporal behavior. The multiple stable states corresponding to the flow histories and initial conditions are physically realizable in Rayleigh-Bénard convection under the Boussinesq approximation. Hof *et al.* [13] conducted experimental research at a small aspect ratio and found that both axisymmetric and asymmetric, stable steady convective structures can exist at the same Rayleigh number for a fixed aspect ratio. Leong [14], Ma *et al.* [15], and Borońska and Tuckerman [16,17] simulate convective flows at the same configuration as Hof *et al.* [13]. Their works verified the various flow patterns in the experiment. Furthermore, Ma *et al.* [15] also observed a stable four-spoke pattern which is not obtained by the experiment. At the same time, Borońska *et al.* [16,17] studied the evolution of the flow patterns with different initial conditions.

However, the pattern formation of Rayleigh-Bénard convection in pure water near 4 °C could be more complex than that in Boussinesq fluid by having the density inversion. The density inversion means that there exists a maximum of the mass density in pure water near 4 °C. Below this temperature, the mass density of pure water increases with the increase of temperature, and it decreases when the temperature is above 4 °C. Until now, very few research activities have focused on convection in confined enclosures submitted to a vertical temperature gradient for cold water. Kalabin *et al.* [18] performed a two-dimensional numerical simulation to study cold water convection near the density maximum in a square cavity heated from below. The vertical walls of the cavity are adiabatic, and the temperature of the top and bottom walls is symmetrical relative to the temperature of the density maximum. When the Grashof number is between 29 000 and 950 000, four steady flow states and three unsteady flow states have been observed. Zubkov *et al.* [19,20] also studied the flow patterns of cold water convection with the same configuration as Kalabin *et al.* [18], and they found six stable flow structures when the Grashof number was between 0 and 17 000. In addition, they determined the existence range of each of the different stable flow states.

The purpose of the present work is to study the pattern formation of Rayleigh-Bénard convection of cold water near its density inversion point in a vertical cylindrical enclosure. Specifically, we will consider the effects of different initial conditions on the convective patterns and multiple stable steady patterns arising within specific ranges of the Rayleigh number. The simulation is conducted under the assumptions of laminar flow and perfectly insulating lateral for a fixed aspect ratio of the enclosure $\Gamma \equiv 2$, which is the same with Ma *et al.* [15] and Borońska *et al.* [16,17], and the range of the Rayleigh numbers is 3000–120 000. We hope to obtain various stable steady patterns in cold water convection near the density inversion point and find out the influence of the density maximum on the flow structures.

*Corresponding author: liyourong@cqu.edu.cn

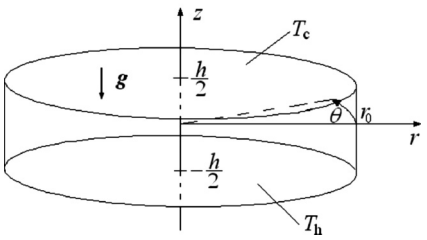

FIG. 1. Sketch of the geometry and coordinate system.

II. PROBLEM FORMULATION

A. Physical and mathematical models

The physical model of the problem is shown in Fig. 1, and the cold water is confined in a cylinder with radius r_0 and depth h. The aspect ratio of the cylinder is defined as $\Gamma = r_0/h = 2$. The upper and lower walls of the cylinder are isothermally kept at constant temperature T_c and T_h ($T_c < T_h$), respectively, and the sidewall is considered to be thermally insulated. All physical properties are taken as constant, except for the density ρ in the buoyancy term, which varies nonlinearly with temperature. The nonlinear temperature-dependent density of water is given as the following form proposed by Gebhart and Mollendorf [21]:

$$\rho(T) = \rho_m(1 - \gamma|T - T_m|^q),$$

where $\rho_m = 999.972\ \mathrm{kg/m^3}$ is the maximum density of water at a temperature $T_m = 4.029\,325\ ^\circ\mathrm{C}$, $q = 1.894\,816$, and $\gamma = 9.297\,173 \times 10^{-6}(^\circ\mathrm{C})^{-q}$.

Using h, ν/h, h^2/ν, and $\rho\nu^2/h^2$ as the reference scales for length, velocity, time, and pressure, respectively, the governing equations in the cylindrical coordinate system can be written in dimensionless form as

$$\nabla \cdot \boldsymbol{V} = 0, \tag{1}$$

$$\partial_t \boldsymbol{V} + \boldsymbol{V} \cdot \nabla \boldsymbol{V} = -\nabla P + \nabla^2 \boldsymbol{V} + (\mathrm{Ra/Pr})|\Theta - \Theta_m|^q \boldsymbol{e_Z}, \tag{2}$$

$$\partial_t \Theta + \boldsymbol{V} \cdot \nabla \Theta = (1/\mathrm{Pr})\nabla^2 \Theta, \tag{3}$$

where $\boldsymbol{V}(V_R, V_\theta, V_Z)$ denotes the dimensionless velocity vector, $\Theta = (T - T_c)/(T_h - T_c)$ the dimensionless temperature, $\Theta_m = (T_m - T_c)/(T_h - T_c)$ the density inversion parameter, and $\boldsymbol{e_Z}$ the unit vector in z direction. In this work, the density inversion parameter is fixed at $\Theta_m = 0.3$. $\mathrm{Ra} = g\gamma\Delta T^q h^3/(\alpha\nu)$ and $\mathrm{Pr} = \nu/\alpha$ are the Rayleigh number and the Prandtl number, respectively, ν is the kinematic viscosity, α the thermal diffusivity, g the gravity acceleration, and ΔT the temperature difference between the top and bottom walls. The Prandtl number Pr of cold water at T_m is about 11.57.

All the container walls satisfy the no-slip boundary condition. Therefore, the dimensionless boundary conditions can be written as follows:

$$Z = 1/2, \quad \Theta = 0, \quad V_R = V_\theta = V_Z = 0, \tag{4}$$

$$Z = -1/2, \quad \Theta = 1, \quad V_R = V_\theta = V_Z = 0, \tag{5}$$

$$R = \Gamma, \quad \partial\Theta/\partial R = 0, \quad V_R = V_\theta = V_Z = 0. \tag{6}$$

TABLE I. Comparison of the average Nusselt number at three different meshes at $\mathrm{Ra} = 4 \times 10^4$.

$N^R \times N^\theta \times N^Z$	$\mathrm{Nu_{ave}}$
$40 \times 120 \times 20$	2.731
$60 \times 160 \times 30$	2.765
$80 \times 200 \times 40$	2.769

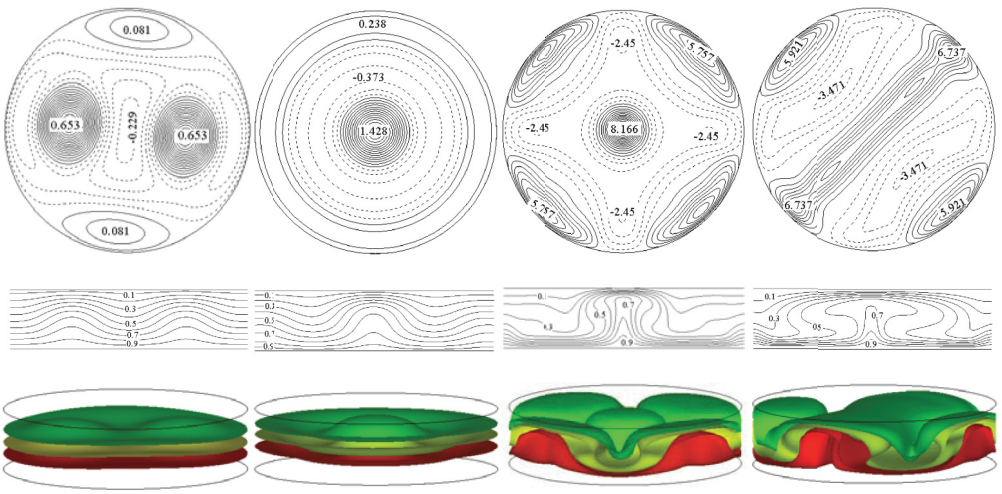

(a) Ra=4102 face (b) Ra=5000 two-tori (c) Ra=40 000 cross dart (d) Ra=47 000 four-roll

FIG. 2. (Color online) Flow patterns at different Rayleigh numbers. Upper plot: Contours of the axial velocity in the $Z = 0$ plane, and dashed lines correspond to negative values. Middle plot: Contours of temperature in the $\theta = 0 - \pi$ plane. Lower plot: Isothermal surfaces of $\Theta = 0.3$ (upper), 0.5 (middle), and 0.7 (lower).

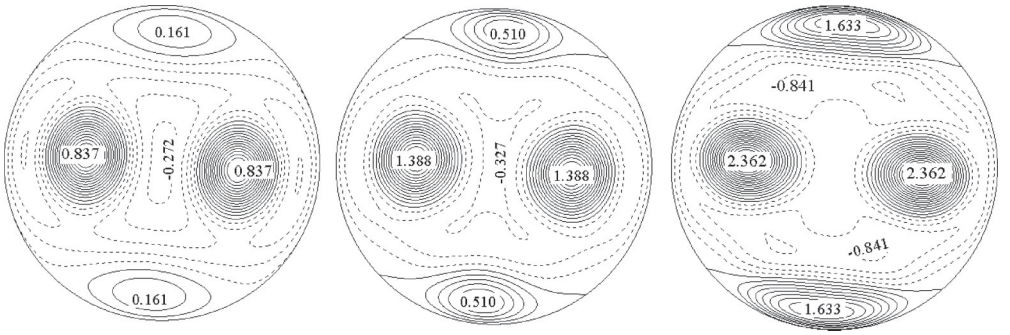

(a) Ra=4300 (b)Ra=5000 (c) Ra=10000

FIG. 3. Flow patterns of stable face states at different Rayleigh numbers.

The average Nusselt number at the hotwall is defined as

$$\mathrm{Nu} = -\frac{1}{2\pi\Gamma}\int_0^{2\pi}\int_0^{\Gamma}\left.\frac{\partial\Theta}{\partial Z}\right|_{Z=-1/2} dRd\theta. \qquad (7)$$

B. Numerical method and validation check

The governing equations (1)–(3) are solved by the finite volume method. The pressure-velocity coupling is handled by using the SIMPLE algorithm, and the diffusion term is approximated by a second-order central difference scheme. For the discretization scheme of the convective term, the QUICK, the second-order upwind and the second-order central schemes were tested. It was found that the pattern formation and the critical Rayleigh number of the flow transition are almost same for the three kinds of schemes. Hence the QUICK scheme is used for the convective term, as shown in Refs. [22–25]. The dimensionless time steps varied from 5×10^{-3} to 1×10^{-4} according to the Rayleigh number and the evolution of flow. At each time step, the solution is considered to be fully converged when the maximum relative errors for velocity and temperature are less than 10^{-5}.

In order to verify the convergence of the grid, independent tests for several different meshes were conducted. As shown in Table I, the average Nusselt number at the hotwall was presented with three different meshes at $\mathrm{Ra} = 4 \times 10^{-4}$. It can be found that a grid size $60^R \times 160^\theta \times 30^Z$ is sufficient for accurate simulation. The present numerical solution has been validated by our previous work [26] for natural convection of cold water in horizontal annulus. Furthermore, due to the lack of research data for Rayleigh-Bénard convection in a vertical cylinder with the presence of cold water, another validation test was conducted for Rayleigh-Bénard convection of water subjected to the Boussinesq approximation in a vertical cylinder with the numerical work of Ma *et al.* [15] and Borońska and Tuckerman [16], as shown in Table II. It is obvious that the present results are in agreement with those in the references.

III. RESULTS AND DISCUSSION

A. Steady flow pattern coming from the conductive state

In the first series of simulations, the flow patterns starting from the conductive state are considered. First of all, we obtained the conductive solution at a small Rayleigh number and then used this conductive solution as the initial condition to run a series of simulations with a variation step of the Rayleigh number from 2 to 200 at a Rayleigh number range between 3800 and 70 000. Depending on the Rayleigh number, several typical flow states are observed as shown in Fig. 2.

If $\mathrm{Ra} < 4102$, the system still remains stationary, that is, the conductive state. For $4102 \leqslant \mathrm{Ra} < 4188$, the final convection state is a steady symmetric pattern. We call this flow pattern the *face* state, as shown in Fig. 2(a). The flow area

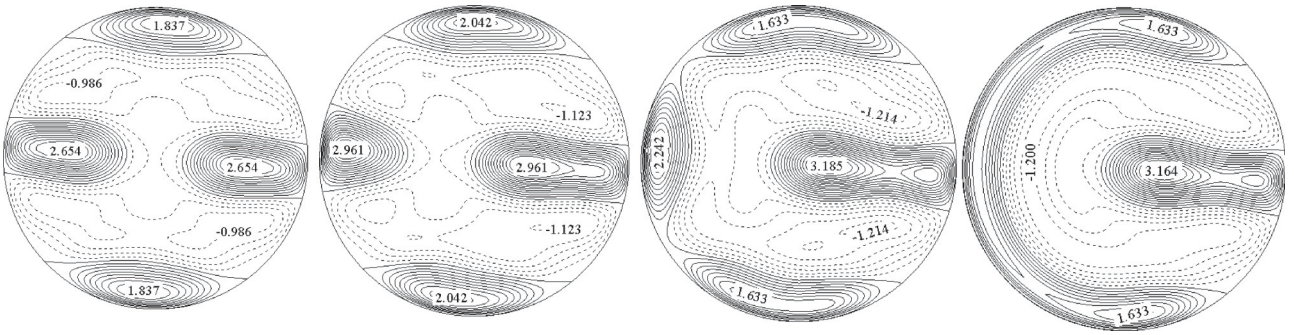

(a) t=0 (b) t= 16.8 (c) t= 56.2 (d) t= 87.5

FIG. 4. Time evolution from face pattern to C pattern at Ra = 11 600.

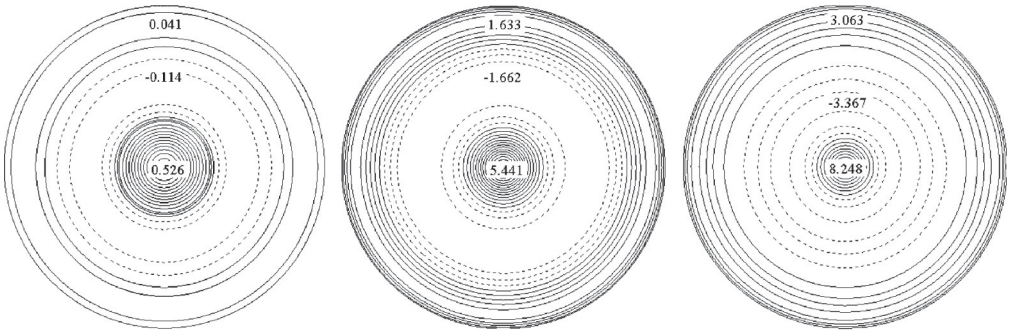

(a) Ra=3950 (b) Ra=18 000 (c) Ra=44 000

FIG. 5. Flow patterns of a stable two-tori state at different Rayleigh numbers.

of this state mainly happened in the center area, with two hot-rising flows and one cold-descending flow, resembling two eyes and a nose in a face. The maximum value of the axial velocity in each up- or down-flow area is also labeled in Fig. 2. For Rayleigh numbers between 4188 and 37 000, the system evolves toward the axisymmetric state, as depicted in Fig. 2(b). This state is named the *two-tori* state because it contains two concentric toroidal rolls, where two hot up-flows rise on the center and boundaries and the cold fluid descends in the middle ring. For $37\,000 \leqslant \mathrm{Ra} < 42\,000$, a *cross-dart* pattern is observed, as shown in Fig. 2(c). This final state has five perfectly separated hot up-flows with one in the center and the others symmetrically distributed near the sidewall. For $42\,000 \leqslant \mathrm{Ra} < 53\,000$, the final pattern consists of four rolls, with two parallel down-flows alternating with three parallel up-flows, thus forming the *four-roll* pattern, as shown in Fig. 2(d). Continuing to increase the Ra number, the system evolves into time-dependent oscillation. For all these patterns mentioned above, the value of axial velocity increases with increase of the Rayleigh number. The isothermal surface in the maximum mass density fluid layer of the different flow pattern is also depicted in Fig. 2.

We find that the convective motion for the entire flow structure mentioned above appears in the whole container when the density inversion parameter $\Theta_m = 0.3$, as shown in the middle plot of Fig. 2. The critical Rayleigh number of Rayleigh-Bénard convection of cold water in the confined cylinder with adiabatic sidewall is a function of not only aspect ratio but also the density inversion parameter. When the aspect ratio $\Gamma = 2$, the critical Rayleigh number in Boussinesq fluids is about 2000, according to the reports of Ma *et al.* [15] and Borońska and Tuckerman [16], and in the present work on cold water, it is near 4100.

TABLE II. Comparison of the critical Rayleigh number at the primary thresholds at $\Gamma = 2$ and $\mathrm{Pr} = 6.7$.

Mode	Ref. [15]	Ref. [16]	Present
$m = 1$	1836	1828.4	1826
$m = 2$	1844	1849.4	1845

B. Evolution from face state

In order to exhibit evolution from the face state, a series of simulations is performed for increasing or decreasing the Rayleigh number with a step of $\Delta\mathrm{Ra}$ between 10 and 200. We used the steady face pattern obtained at $\mathrm{Ra} = 4150$ as the initial condition to start the calculation. Furthermore, during the simulations, the initial condition of the next simulation is the result of the last simulation. When the Rayleigh number is below 3940, the face pattern decays to the conductive state. This result shows that there exists a hysteresis for the first flow pattern transition of cold water convection, since we reported earlier that the conductive state does not lose its stability until the Rayleigh number is increased above 4102. For $3940 \leqslant \mathrm{Ra} \leqslant 11\,500$, the face pattern remains stable. With the increase of the Rayleigh number, the hot up-flow near the sidewall becomes much stronger, the absolute maximum value of axial velocity in these areas gradually exceeds the absolute maximum value of axial velocity in the cold down-flow, and the two up-flows in the center move slowly to the boundaries, as shown in Fig. 3. When $\mathrm{Ra} = 11\,600$, the face pattern finally transforms into a stable C state by passing through several intermediate patterns, as shown in Fig. 4.

In the results of Ma *et al.* [15] and Borońska *et al.* [16], who obtained numerically a rich variety of flow states with Boussinesq approximation, the first bifurcation pattern is the dipole state instead of the face state. However, in the cold water convection, it is found that the dipole state is an intermediate

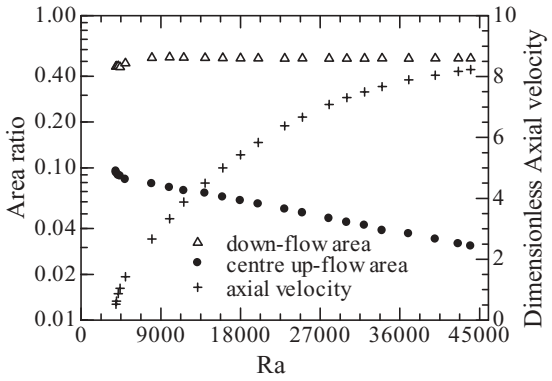

FIG. 6. The maximum axial velocity in center flow and flow area ratio as a function of Rayleigh number.

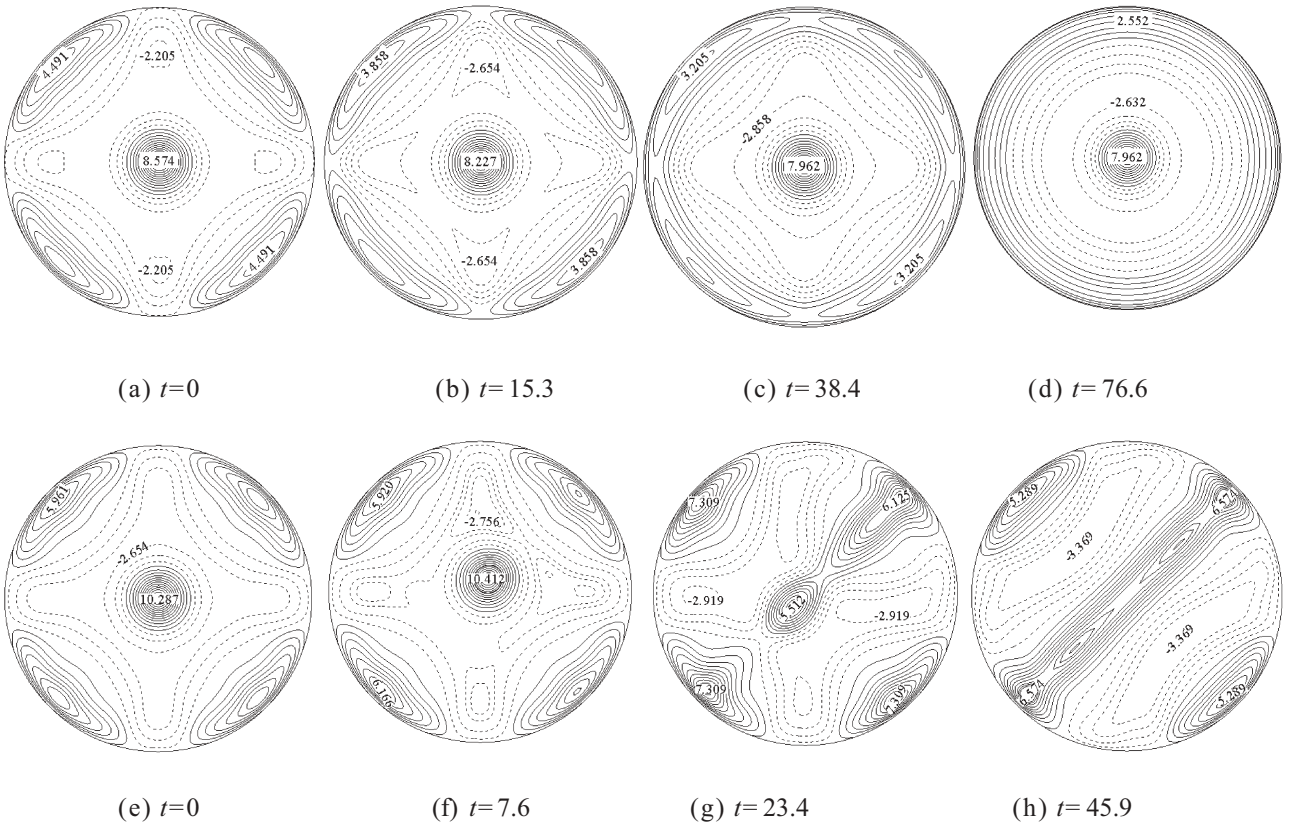

(a) t=0 (b) t= 15.3 (c) t= 38.4 (d) t= 76.6

(e) t=0 (f) t= 7.6 (g) t= 23.4 (h) t= 45.9

FIG. 7. Time evolution from cross-dart structure: (a)–(d) Ra = 31 000, (e)–(h) Ra = 47 200.

pattern when the face pattern decays into a conductive state.

C. Evolution from axisymmetric state

In this simulation we used the axisymmetric *two-tori* state converged at 5000, like that in Fig. 2(b), as the initial condition. When 3950 $\leqslant$ Ra $\leqslant$ 44 600, the *two-tori* pattern is stable, as shown in Fig. 5. The convection is enhanced with the increase of the Rayleigh number. The maximum absolute axial velocity in the center upwelling fluids is always stronger than that in the descending fluids. Figure 6 shows the value of the maximum axial velocity in the center up-flow. Furthermore, the flow area ratio of the center hot up-flow to the whole midplane and the area ratio of the cold down-flow to the midplane at different Rayleigh numbers are also shown in Fig. 6, respectively. With the increase of the Rayleigh number, the flow areas of the center up-flow decrease and the flow areas of the cold down-flow nearly keep constant after a small increase at low Rayleigh numbers. The total flow area of the hot upwelling fluids is a little smaller than that of the cold-descending area when the flow area of the down-flow reaches a constant, and this phenomenon exactly satisfies the continuity requirement that the mass flow rate of the hot upwelling fluids must be the same with the cold-descending fluids, in view of the smaller absolute axial velocity in the cold-descending area. For Ra < 3950, the two-tori state transforms into the conductive state, and for the Rayleigh number

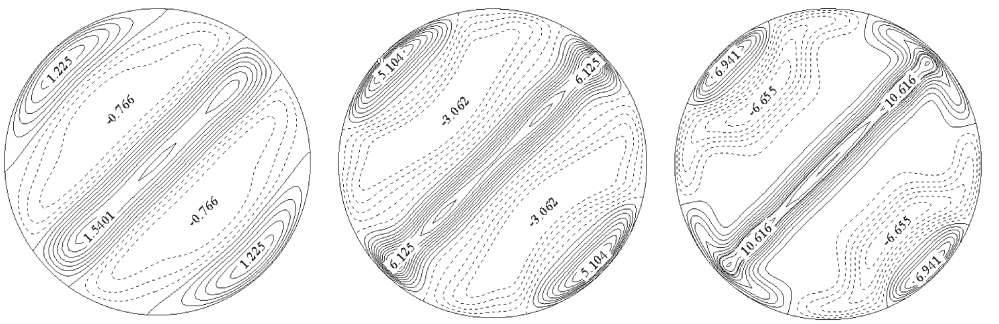

(a) Ra=7600 (b) Ra= 39 00 (c) Ra=10000

FIG. 8. Flow patterns of stable four-roll states at different Rayleigh numbers.

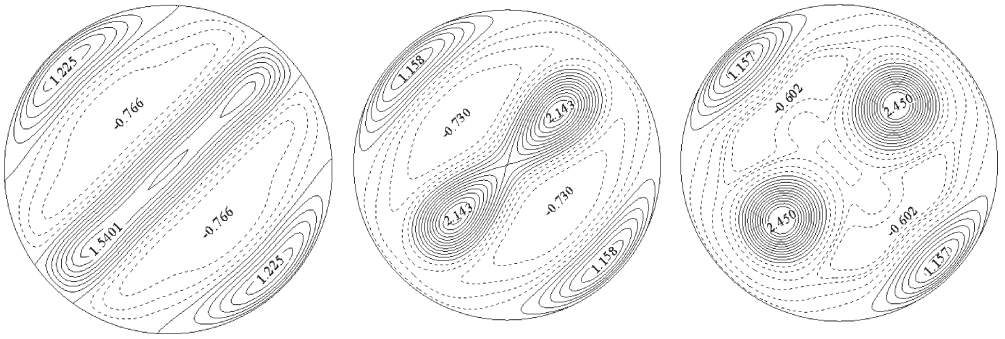

(a) t=0 (b) t=31.2 (c) t=91.8

FIG. 9. Time evolution from four-roll structure to stable face structure at Ra = 7400.

above 44 600, the stable, steady two-tori pattern evolves into oscillation.

D. Evolution from cross-dart state

The space structure of the cross-dart pattern is similar to the four-spoke pattern observed by Ma *et al.* [15]. Both of the two states contain four hot upwelling areas near the sidewall, which is separated symmetrically by the cold downwelling fluids. However, for the cross-dart pattern, the center of the cylinder is held by hot upward fluids, which is different with the four-spoke pattern. For the stable cross-dart pattern, we used the result converged at Ra = 40 000, as shown in Fig. 2(c), as the initial condition. The simulation results indicate that this kind of steady flow structure exists in the range of Rayleigh numbers 31 600 $\leqslant$ Ra $\leqslant$ 47 000, and for Ra $<$ 31 600 it transforms into the stable axisymmetric state, as shown in Figs. 7(a)–7(d); for Ra $>$ 47 000, it leads to the stable four-roll state, as shown in Figs. 7(e)–7(h).

E. Evolution from the four-roll state

This time we used the stable four-roll state converged at Ra = 47 000, as shown in Fig. 2(d), as the initial condition. It is found that the four-roll state is stable for a very wide range of Rayleigh numbers, 7600 $\leqslant$ Ra $\leqslant$ 110 000. As in the case of Boussinesq fluid reported by Borońska and Tuckerman [16], the roll becomes more curved and the roll boundaries grow much thinner with the increase of Rayleigh number, as shown in Fig. 8. For Ra = 7400, the four-roll flow leads to the *face* state, as displayed in Fig. 9. When the Rayleigh number exceeds 110 000, the steady state loses stability and transforms into a time-dependent flow.

F. Evolution from a stable C state

The initial condition used here is the stable C state, as shown in Fig. 4(d), obtained previously at Ra = 11 000. For Rayleigh numbers between 9000 and 23 000, we found this kind of pattern still to be stable, as shown in Fig. 10(a). We also found that the roll becomes more curved and the flow boundaries become much thinner with the increase in Rayleigh number. For 4600 $\leqslant$ Ra $<$ 9000, the new evolved states are also of the C family, but the flow patterns have some changes. For 6500 $\leqslant$ Ra $<$ 9000, the new state is the *four-spot* pattern; the curved hot up-flow near the sidewall in C pattern splits into four

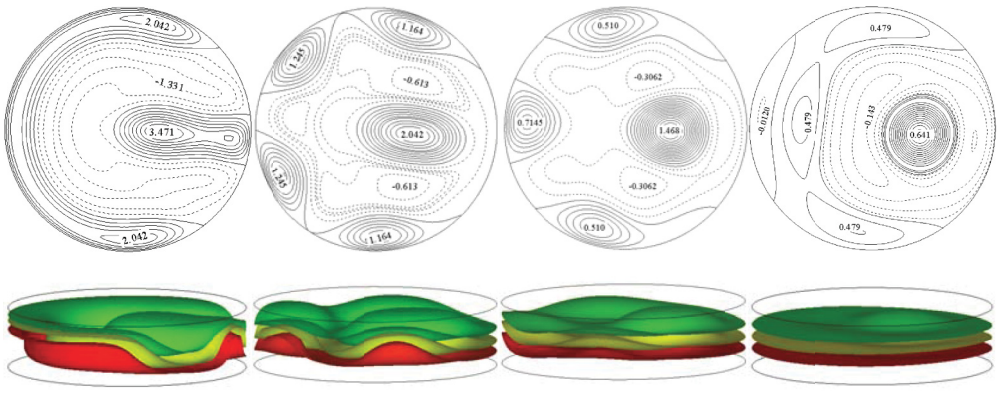

(a) Ra=14000 (b) Ra=7000 (c) Ra=5000 (d) Ra=4000

C four-spot three-spot deformity

FIG. 10. (Color online) Flow patterns and isothermal surfaces of stable C family at different Rayleigh numbers: Θ = 0.3 (upper), 0.5 (middle), and 0.7 (lower).

TABLE III. Stability range of all stable, steady convective patterns.

Flow pattern name	Corresponding figure	Range of stability
Face	Fig. 2(a)	$3940 \leqslant \mathrm{Ra} \leqslant 11500$
Deformity	Fig. 10(d)	$3946 \leqslant \mathrm{Ra} \leqslant 4050$
Two-tori	Fig. 2(b)	$3950 \leqslant \mathrm{Ra} \leqslant 44600$
Three-spot	Fig. 10(c)	$4600 \leqslant \mathrm{Ra} < 6500$
Four-spot	Fig. 10(b)	$6500 \leqslant \mathrm{Ra} < 9000$
C	Fig. 4(d)	$9000 \leqslant \mathrm{Ra} \leqslant 23000$
Cross dart	Fig. 2(c)	$31600 \leqslant \mathrm{Ra} \leqslant 47000$
Four-roll	Fig. 2(d)	$7600 \leqslant \mathrm{Ra} \leqslant 110000$

completely independent flow areas, as shown in Fig. 10(b). For $4600 \leqslant \mathrm{Ra} < 6500$, the C pattern flow changes into the *three-spot* pattern, with the hot fluids rising on three spot areas along the boundaries, as shown in Fig. 10(c). For $4600 < \mathrm{Ra} \leqslant 4050$, the stable C pattern transforms into the stable face pattern, and for $3946 < \mathrm{Ra} \leqslant 4050$, it evolves into a new nonsymmetric pattern, as shown in Fig. 10(d). The convection motion in this structure happened mainly on one side of the cylinder and the flow on the rest is very weak. Therefore we named this pattern the *deformity* pattern. When $\mathrm{Ra} > 23\,000$, the stable C flow leads to a period oscillation with a constant amplitude.

G. Summary

Table III gives the stability range of all stable steady patterns that we have obtained. The average Nusselt number at the hotwall as a function of Rayleigh number is shown in Fig. 11. For lower Rayleigh numbers, we obtained three stable steady patterns: face, two-tori, and deformity. For higher Rayleigh numbers, two types of flow patterns are still stable over large intervals of the Rayleigh number: two-tori and four-roll patterns. The average Nusselt number depends primarily on the Rayleigh number and is slightly influenced by the flow pattern.

The pattern formation in cold water is different from that in the Boussinesq fluids reported by Borońska *et al.* [16]. For higher Rayleigh numbers and perfectly adiabatic sidewalls, we observed two-tori, four-roll, and cross-dart patterns in cold water convection. However, according to Borońska *et al.* [16], they obtained six stable flow patterns, and none of the flow patterns observed near the onset of the convection seem to be stable at higher Rayleigh numbers. On the contrary, the two-tori pattern in cold water convection can exist in a wide range of Rayleigh numbers, from 3950 to 44 600.

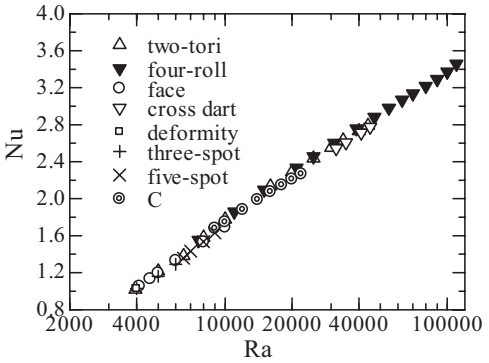

FIG. 11. Variation of the average Nusselt number at the hotwall.

IV. CONCLUSIONS

Rayleigh-Bénard convection of cold water near its density maximum in a vertical cylindrical enclosure heated from below has been studied with a fully three-dimensional numerical simulation. The aspect ratio of the cylinder was $\Gamma = 2$, matching the geometry of Ma *et al.* [15] and Borońska *et al.* [16], who obtained numerically a rich variety of flow patterns with the Boussinesq approximation. The following conclusions were obtained:

(1) For the range of Rayleigh numbers between 3000 and 110 000, eight stable steady convection patterns were obtained. Even close to the threshold (at $\mathrm{Ra} = 4100$) we found three stable patterns: deformity, face, and two-tori patterns. Furthermore, the coexisting phenomenon of the steady axisymmetric structure and nonaxisymmetric structure within specific ranges of Rayleigh numbers in cold water convection also is observed.

(2) For the buoyancy convection of cold water near its maximum density, our research demonstrates that the initial condition has a significant effect on the form of the convection structure.

(3) While determining the stability of the various stable patterns, a hysteresis phenomenon was observed, which is not reported in the reports of Ma *et al.* [15] and Borońska *et al.* [16,17]. This phenomenon, however, has an important influence on the stability range of various convective patterns.

ACKNOWLEDGMENTS

This work was supported by the National Natural Science Foundation of China (Grant No. 50976129) and the Research Fund for the Doctoral Program of Higher Education of China (Grant No. 20110191110015).

[1] K. Stork and U. Müller, J. Fluid Mech. **71**, 231 (1975).
[2] G. Müller, G. Neumann, and W. Weber, J. Cryst. Growth **70**, 78 (1984).
[3] R. V. Cakmur, D. A. Egolf, B. B. Plapp, and E. Bodenschatz, Phys. Rev. Lett. **79**, 1853 (1997).
[4] F. Hébert, R. Hufschmid, J. Scheel, and G. Ahlers, Phys. Rev. E **81**, 046318 (2010).
[5] S. Rosenblat, J. Fluid Mech. **122**, 395 (1982).
[6] J. C. Buell and I. Catton, J. Heat Transfer **105**, 255 (1983).
[7] M. C. Cross and P. C. Hohenberg, Rev. Mod. Phys. **65**, 851 (1993).
[8] G. Neumann, J. Fluid Mech. **214**, 559 (1990).
[9] M. Wanschura, H. C. Kuhlmann, and H. J. Rath, J. Fluid Mech. **326**, 399 (1996).

[10] R. Touihri, H. Ben Hadid, and D. Henry, Phys. Fluids **11**, 2078 (1999).
[11] S. Rüdiger and F. Feudel, Phys. Rev. E **62**, 4927 (2000).
[12] G. Silano, K. R. Sreenivasan, and R. Verzicco, J. Fluid Mech. **662**, 409 (2010).
[13] B. Hof, G. J. Lucas, and T. Mullin, Phys. Fluids **11**, 2815 (1999).
[14] S. S. Leong, Numer. Heat Transfer, Part A **41**, 673 (2002).
[15] D. J. Ma, D. J. Sun, and X. Y. Yin, Phys. Rev. E **74**, 037302 (2006).
[16] K. Borońska and L. S. Tuckerman, Phys. Rev. E **81**, 036320 (2010).
[17] K. Borońska and L. S. Tuckerman, Phys. Rev. E **81**, 036321 (2010).
[18] E. V. Kalabin, E. M. Sviridov, and P. T. Zubkov, Heat Transfer Sci. Technol. **2000**, 217 (2000).
[19] P. T. Zubkov and E. V. Kalabin, Fluid Dyn. **36**, 944 (2001).
[20] P. T. Zubkov, E. V. Kalabin, and A. V. Yakovlev, Fluid Dyn. **37**, 847 (2002).
[21] B. Gebhart and J. C. Mollendorf, Deep-Sea Res. **24**, 831 (1977).
[22] I. Sezai and A. A. Mohamad, Phys. Fluids **12**, 432 (2000).
[23] N. Y. Zhan, M. Yang, Z. Y. Wang, L. Li, and Z. Z. Zheng, Prog. Comput. Fluid Dyn. **8**, 526 (2008).
[24] E. H. Ridouane, A. Campo, and J. Y. Chang, Int. J. Numer. Methods Fluids **56**, 453 (2008).
[25] D. K. Maiti, A. S. Gupta, and S. Bhattacharyya, J. Heat Transfer **130**, 122001 (2008).
[26] Y. R. Li, X. F. Yuan, C. M. Wu, and Y. P. Hu, Int. J. Heat Mass Transfer **54**, 2550 (2011).